AJPR
Avicenna Journal of Pharmaceutical Research
Avicenna J Pharma Res. 2025 ;6(2): 88-98
DOI: 10.53208/ajpr.6.2.88
http://ajpr.umsha.ac.ir

Original Article

PLLA/Alen@β-CD@Fe-MIL88B Scaffold for Bone Regeneration: Fabrication, Characterization, and In Vitro Evaluation

Azadeh Golmohamadpour[1], Gebremariam Birhanu Wondie[2,3], Alireza Lotfabadi[4], Mehdi Doosti-Telgerd[5,6*]

[1] College of Chemistry, Shahrood University of Technology, Shahrood, Iran
[2] Department of Pharmaceutics and Social Pharmacy, School of Pharmacy, College of Health Sciences, Addis Ababa University, Addis Ababa, Ethiopia
[3] Department of Pharmacology, Faculty of Health Sciences, University of the Free State, Bloemfontein 9300, South Africa.
[4] Pharmaceutical Sciences Research Center, Health Institute, Kermanshah University of Medical Sciences, Kermanshah, Iran
[5] Department of Pharmaceutics, School of Pharmacy, Hamadan University of Medical Sciences, Hamadan, Iran
[6] Medicinal Plants and Natural Products Research Center, Institute of Cancer, Hamadan University of Medical Sciences, Hamadan, Iran

Article history:
Received: September 11, 2025
Revised: September 20, 2025
Accepted: October 13, 2025
ePublished: February 10, 2025

***Corresponding author:**
Mehdi Doosti-Telgerd, Department of Pharmaceutics, School of Pharmacy, Hamadan University of Medical Sciences, Hamadan, Iran.
Medicinal Plants and Natural Products Research Center, Institute of Cancer, Hamadan University of Medical Sciences, Hamadan, Iran.
Email: m-dusti@alumnus.tums.ac.ir

Abstract

Background: Repairing damaged bone tissue remains a major clinical challenge. Tissue engineering offers a promising solution, requiring scaffolds that support cell growth while delivering therapeutic molecules in a controlled manner. This study aimed to develop a novel composite scaffold for bone tissue engineering using a biodegradable polymer and drug-loaded metal-organic framework particles.

Methods: We fabricated fibrous scaffolds via electrospinning using poly-L-lactic acid (PLLA) and iron-based metal-organic framework particles (Fe-MIL-88B-NH_2). The particles were functionalized with β-cyclodextrin and loaded with the bone-active drug alendronate. The drug carrier was characterized using scanning electron microscopy (SEM), X-ray diffraction, and infrared spectroscopy. The loaded particles were then incorporated into the polymer solution to produce electrospun scaffolds. Drug release was evaluated in a simulated body fluid. Furthermore, human adipose-derived mesenchymal stem cells were cultured on the scaffolds, and their osteogenic behavior was assessed via alkaline phosphatase activity, calcium deposition, and MTT metabolic assays.

Results: The drug carriers were successfully synthesized and characterized. The composite scaffolds released alendronate significantly slower than free drug carriers, demonstrating that the polymer network effectively controlled drug release over time. Biological assays revealed that scaffolds containing the drug-loaded particles were more effective than plain PLLA scaffolds in promoting bone-related cell activity and improving surface properties.

Conclusion: Combining the carrier system with alendronate in the electrospun PLLA matrix enhanced osteogenic activity, successfully driving stem cells toward bone-forming cells.

Keywords: Bone Tissue Engineering; Electrospinning; Metal-Organic Frameworks; Alendronate; Drug Delivery Systems.

Introduction

Orthopedic practice today faces a substantial obstacle in the healing of bone defects, a problem intensified by the widespread occurrence of skeletal illnesses and structural deformities across diverse age groups. While traditional reparative techniques are still frequently applied, they are not without inherent shortcomings, such as restricted availability of donor tissue, donor-site morbidity, and unfavorable postoperative events [1]. These factors have steered research endeavors toward tissue-engineered solutions as a promising alternative. At the heart of these strategies lies the scaffold, which acts as a foundational framework enabling cells to anchor, proliferate, and migrate

© 2025 The Author(s); Published by Hamadan University of Medical Sciences. This is an open-access article distributed under the terms of the Creative Commons Attribution License (http://creativecommons.org/licenses/by/4.0), which permits unrestricted use, distribution, and reproduction in any medium, provided the original work is properly cited.

[Downloaded from ajpr.umsha.ac.ir on 2026-11-15]

[DOI: 10.53208/ajpr.6.2.88]

through the construct [2, 3]. Of the various scaffold types, those possessing nanofibrous architecture stand out prominently, given their capability to emulate the native extracellular matrix and generate a spatially organized three-dimensional setting conducive to cellular performance and regenerative outcomes [3].

Poly-L-lactic acid (PLLA), a synthetic polymer bearing FDA approval, finds widespread utility across diverse biomedical domains, including tissue engineering and controlled drug administration. Its appeal in the fabrication of bone tissue scaffolds stems from favorable attributes, namely biodegradability, biocompatibility, and remarkable processability in generating various architectural forms. Nevertheless, certain shortcomings have curtailed its standalone application in skeletal repair, among them inadequate bioactivity, suboptimal mechanical resilience, generation of acidic degradation products, and a propensity to incite inflammatory host reactions [4]. Given that PLLA-based constructs tend toward flexibility, whereas inorganic materials like ceramics and bioglasses are characterized by excessive rigidity and fragility, a compelling rationale has emerged for the design of composite systems that synergistically combine distinct material classes. Concurrently, the incorporation of osteoinductive agents—including growth factors and pharmacologically active molecules—into scaffold matrices has garnered attention as a means to expedite regenerative events. Against this backdrop, current investigative trajectories increasingly favor composite scaffolds impregnated with therapeutic moieties, functioning as localized depots that ensure sustained bioactive molecule release directly at lesioned sites, thereby facilitating bone neoformation [5]. By way of illustration, previous findings indicate that dexamethasone eluted from bioactive glass phases embedded within PLLA nanofibers can effectively promote odontogenic differentiation in dental pulp-derived cells [6].

Metal-organic frameworks (MOFs) constitute an emerging class of highly porous crystalline architectures, wherein inorganic nodes are coordinatively bridged by organic spacer ligands. Over the past two decades, this family of materials has attracted considerable scholarly attention, with investigative efforts spanning diverse technological fronts, including gaseous hydrocarbon entrapment [7], adsorptive separation processes [8, 9], heterogeneous catalysis [10], and contrast-enhanced magnetic resonance imaging [11, 12]. More recently, their application portfolio has expanded to encompass pharmaceutical delivery systems [13]. The intrinsic porosity of MOFs renders them suitable hosts for a variety of low-molecular-weight cargoes, ranging from simple diatomic gases [14] to chemotherapeutic agents such as fluorouracil and mitoxantrone, as well as antiviral compounds like azidothymidine triphosphate. A substantial body of research has been directed toward optimizing both payload capacity and release kinetics, with functionalization strategies—including the incorporation of amino moieties [14] or macrocyclic oligosaccharides such as cyclodextrins—representing prominent approaches to modulate host–guest interactions and fine-tune elution behavior.

Alendronate (Alen), classified as a third-generation bisphosphonate agent, has garnered substantial research interest owing to its distinctive multifunctional profile. This compound exerts a dual osteogenic influence by both promoting osteoblast lineage commitment and maturation [15], while simultaneously inducing programmed cell death in osteoclasts [16, 17], thereby tilting the balance of bone remodeling toward net formation. Beyond its skeletal metabolic effects, alendronate exhibits a noteworthy differential affinity for neoplastic bone tissue relative to its healthy counterpart, a property that renders it particularly attractive for targeted therapeutic interventions directed at osseous malignancies [18]. Collectively, these inherent attributes position alendronate not merely as an anti-resorptive agent, but as a versatile molecular tool with potential applications in both regenerative strategies and site-specific drug delivery to pathological bone microenvironments.

In this study, through direct mixing of 2-aminoterephthalic acid and ferric chloride in the presence of pluronic F127 and acetic acid, the Fe-

[Downloaded from ajpr.umsha.ac.ir on 2026-11-15]

[DOI: 10.53208/ajpr.6.2.88]

MIL-88-NH2 nano-carriers were synthesized. Subsequently, the β-cyclodextrin was used for nanoparticles' surface modification to increase Alen loading. After the loading process, β-CD@Fe-MIL-88B nano-carriers and Alen-loaded β-CD@Fe-MIL-88B nano-carriers (Alen@β-CD@Fe-MIL88B) were incorporated in a PLLA-based scaffold. It is hypothesized that incorporation of Alen@β-CD@Fe-MIL88B into a PLLA-based scaffold would reduce the release rate of Alen. The resulting scaffold was subsequently evaluated for its ability to improve the osteogenic activity of human adipose tissue-derived mesenchymal stem cells (hASCs) in an in vitro model.

Materials and Methods

Synthesis of nanoparticles

Synthesis of Fe-MIL-88B-NH_2

The NPs were synthesized according to the method reported previously by Golmohamadpour et al. [19]. The reaction mixture for the synthesis of Fe-MIL-88B-NH_2 NPs consisted of F127 (0.32 g), $FeCl_3$. $6H_2O$ (0.66 mmol), CH_3COOH (0.75 ml), NH_2-BDC (0.33 mmol) and deionized water (DW) (26.7 ml) in a molar ratio of 0.04:1:4:0.5:1255. The mixture was transferred to a Teflon-lined stainless-steel autoclave and heated at 110°C for 24 h. In the next step, the reaction vessel was slowly cooled down to room temperature (RT), and the resulting product was filtered, washed with ethanol, and dried.

Synthesis of β-CD functionalized Fe-MIL-88B (β-CD@Fe-MIL-88B)

This was a two-step process. First, Tosylated β-CD was synthesized, introducing dissolved NaOH (164 mmol, 6.56 g) in 20 ml DW to the β-CD (52.8 mmol, 60 g) suspension in 500 ml DW. Afterward, p-toluenesulfonyl chloride (p-TsCl) (52.8 mmol, 10 g) solution in 30 ml acetonitrile was added dropwise over 30 min and then stirred for an additional 2 h. The obtained mixture was filtered and acidified to pH 2–3 with 1 M HCl, and then kept in the refrigerator overnight. Tosylated β-CD (Ts- β-CD) was obtained by washing and drying the filtered precipitate at RT. The next step included functionalizing the synthesized Fe-MIL-88B surface with obtained β-CD (Ts- β-CD), in which Fe-MIL-88B-NH2 (200 mg) suspension in dry DMF (50 ml) was stirred for 30 min following adding dry triethylamine (Et_3N, 1 mmol, 0.1 g) and sonicating for 30 min. Finally, Ts- β-CD (1 mmol, 1.134 g) was introduced to the obtained mixture stirring overnight. The synthetic powder was rinsed and vacuum-dried at RT for 12 h to access β-CD functionalized Fe-MIL-88B nano-carrier (β-CD@Fe-MIL-88B).

Loading alendronate to β-CD@Fe-MIL-88B (Alen@β-CD@Fe-MIL88B)

Alen@β-CD@Fe-MIL88B was prepared by mixing β-CD@Fe-MIL-88B (100 mg) with alendronate sodium (3 mmol, 0.975 g) and NaCl (50 ml, 0.029 g, 0.01 N). The mixture was stirred continuously for 3 days. The precipitate was separated by centrifugation and washed with water. Subsequently, the product was separated, washed, and dried under vacuum at RT for 24 h.

Drug encapsulation and loading efficiencies

To evaluate the amount of encapsulated drug, the dialysis bag containing the suspension of Alen@β-CD@Fe-MIL-88B (10 mg) with PBS (3 ml) was kept stirring for 28 days, and specific amounts of samples were drawn. The obtained supernatants were collected, and alendronate content was assessed using an established indirect method based on ninhydrin-mediated derivatization and subsequent UV-Vis spectrophotometric analysis. Loading capacity (ILC, %) and loading efficiency (ILE, %) were calculated according to formulae (1) and (2), respectively:

$$\text{Alendronate loading efficiency (ILE, \%)} = \frac{\text{Weight of the loaded alendronate}}{\text{Weight of the initial alendronate}} \times 100 \quad (1)$$

$$\text{Alendronate loading capacity (ILC, \%)} = \frac{\text{Weight of the loaded alendronate}}{\text{Weight of the final product}} \times 100 \quad (2)$$

[Downloaded from ajpr.umsha.ac.ir on 2026-11-15]

[DOI: 10.53208/ajpr.6.2.88]

Scaffold fabrication Method

Pristine PLLA (Sigma-Aldrich), β-CD@Fe-MIL88B-loaded PLLA and Alen@β-CD@Fe-MIL88B-loaded PLLA scaffold were fabricated through electrospinning. Electrospinning was carried out using a horizontal dual-nozzle setup (24-gauge needles), under the following fixed conditions: flow rate of 0.5 mL/h, working distance of 15 cm, voltage of 18 kV, and collector rotational speed of 400 rpm. All scaffold types were prepared under identical parameter settings to maintain processing consistency [20].

Preparation of PLLA, PLLA/β-CD@Fe-MIL88B and PLLA/Alen@β-CD@Fe-MIL88B solution

A 7% w/v PLLA solution was prepared by dissolving 0.43 g of polymer in 6.0 mL of chloroform (Merck) under constant stirring, followed by the addition of 1.0 mL of DMF to obtain a clear homogeneous mixture, which was subsequently used for electrospinning of scaffolds.

For the preparation of composite scaffolds, the β-CD@Fe-MIL88B and Alen@β-CD@Fe-MIL88B were first dispersed in 1.0 mL of DMF and then combined with the PLLA solution in chloroform, yielding a uniform suspension ready for electrospinning [20].

Characterization of β-CD@Fe-MIL88B NPs, Alen@β-CD@Fe-MIL88B NPs and PLLA/Alen@β-CD@Fe-MIL88B

The FT-IR spectra of Fe-MIL88B-NH_2, β-CD@Fe-MIL-88B and Alen@β-CD@Fe-MIL-88B were recorded on a Magna-IR 550 FT-IR spectrometer (Nicolet, USA) with the KBr pellet method. Scanning electron microscopy (SEM; Tuscan/Mira, Czech Republic) was used to observe the morphology of both the synthesized Alen@β-CD@Fe-MIL88B NPs and the Alen@β-CD@Fe-MIL88B-loaded PLLA scaffold. For imaging, all samples were fixed onto an aluminum stub and were coated with a thin layer of gold. The crystalline structure of the Fe-MIL-88B-NH_2 and Alen@β-CD@Fe-MIL88B was analyzed using an X-ray diffraction technique with a PANalytical X'Pert-Pro instrument.

Release study

In vitro release behavior of Alen from Alen@β-CD@Fe-MIL88B-loaded PLLA scaffold

The in vitro release of Alen from the Alen@β-CD@Fe-MIL88B-loaded PLLA scaffold was assessed by incubating the composite scaffold in 2 mL of PBS at pH 7.4 and 37°C in a shaking incubator. A 2 mL aliquot was collected at each designated time point and replenished the solution with 2 mL of fresh PBS.

Colorimetric assessment of drug content was performed by mixing 1 mL of the release sample with 0.5 mL of $NaHCO_3$ aqueous solution (0.5 M, Sigma-Aldrich) and 2.5 mL of ninhydrin solution (2 mg/mL). The blend was incubated at 90°C for 30 min, generating a violet-blue coloration. Absorbance measurements were subsequently taken at 568 nm using a UV-Vis spectrophotometer (Shimadzu UV-VIS) [21].

In vitro studies

Cell proliferation assay

Cell attachment and proliferation were assessed by placing circular scaffolds (1.5 mm diameter) in culture plates, sterilizing with 70% ethanol, and washing twice with PBS prior to incubation with basal medium (DMEM supplemented with 10% FBS). Each scaffold received a seeding density of 5×10^3 cells.

Osteogenic differentiation

For osteogenic differentiation studies, scaffolds received cell seeding at a density of approximately 10^4 cells/cm² and were cultured until ~80% confluence was achieved. Differentiation was then induced by supplementing the basal medium with 0.2 mM ascorbic acid 2-phosphate (Sigma-Aldrich), 10 mM β-glycerophosphate (Sigma-Aldrich), and 100 nM dexamethasone (Sigma-Aldrich).

Alkaline Phosphatase (ALP) activity

ALP activity was assessed using a colorimetric kit (Parsazmoon, Tehran, Iran) on days 7 and 14. Protein extraction was performed with radioimmunoprecipitation assay (RIPA) buffer (250 mL) supplemented with protease inhibitors to prevent degradation. Lysates were shaken at

[Downloaded from ajpr.umsha.ac.ir on 2026-11-15]

[DOI: 10.53208/ajpr.6.2.88]

4°C for 1 h and centrifuged at 15,000 rpm for 15 min. Afterwards, 20 µL of supernatant was reacted with p-nitrophenyl phosphate (ALP enzyme-substrate), producing a yellow color. ALP activity (IU/L) was normalized to the total protein content (mg/dL), measured at 570 nm.

Calcium content

Calcium deposition was evaluated on days 7 and 14 using a commercial assay kit (Parsazmoon, Tehran, Iran). Scaffolds (with and without cells) were homogenized in 0.6 N HCl, shaken at 4°C for 1 h to extract calcium, and quantified following the kit's instructions using serially diluted standards.

Statistical analysis

The resulting data were presented as mean ± standard deviation from at least three independent experiments. Statistical analysis was performed using two-way ANOVA, and significance was defined as $p < 0.05$.

Results and Discussion

NPs characterization

FTIR

The FT-IR spectra of Fe-MIL-88B-NH_2, β-CD@Fe-MIL-88B, and Alen@β-CD@Fe-MIL-88B in an activated state and CO_2 atmosphere are shown in Figure 1 The FT-IR spectrum of Fe-MIL-88B-NH2 and β-CD@Fe-MIL-88B showed two characteristic symmetric and asymmetric stretching bands of primary amine groups appeared at 3300 and 3400cm^{-1} region. Observing no band at around 1700 cm^{-1} suggests that protonated carboxylic groups of utilized acetic acid are absent in the synthesis. The binding of 2-aminoterphtalic acid ligands to the iron salt resulted in the characteristic Fe–O band at 525 cm^{-1}.

The wide typical characteristic band of O-H stretching vibration of β-cyclodextrin is typically observed at 3349 cm^{-1}, while here, because of overlapping with amine groups of the MOF it was not clearly resolved.

For β-CD@Fe-MIL-88B, new characteristic peaks at 1560 and 1660 cm^{-1} may arise from the interactions between primary aromatic amine of the MOF and OH group of β-cyclodextrin, resulting in creating the new NH-O band. In addition, the typical stretching and bending vibration of C-H bond are located at 2935 and 1498 $cm^{-1,}$ while the coupling of the vibrational bands of C-O, C-C, and C-O-H are represented at 1117 cm^{-1}. The weak peak at 966 cm^{-1} is due to the α-1, 4 linkages of the β-CD skeletal.

Alendronate exhibited characteristic bands associated with P=O and C–O bonds in the 900–1200 cm^{-1} region. The shoulder at 1264 cm^{-1} is related to the P=O asymmetric bond, while the respective stretching vibration of P-O is demonstrated at 1060 and 1132 cm^{-1}. The P-OH asymmetric band is illustrated at 1000 cm^{-1} with a shoulder. The peaks at 3411 and 3236 cm^{-1} are attributed to the characteristic N-H stretching vibration, while the ones at 1540 and 1638 cm^{-1} are related to the bending vibrations.

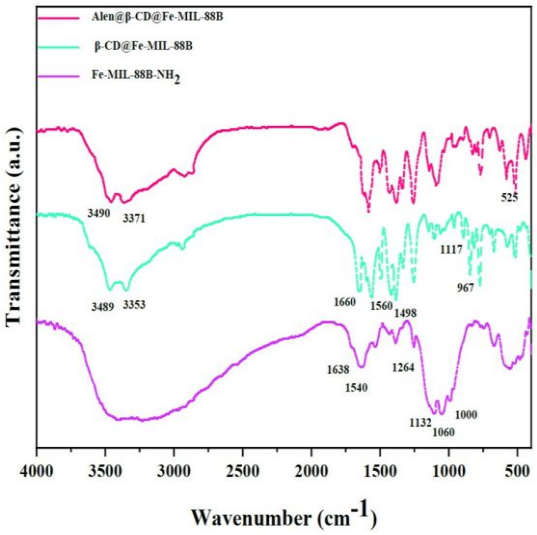


Figure 1. FT-IR spectra of Fe-MIL-88B-NH_2, β-CD@Fe-MIL-88B and Alen@β-CD@Fe-MIL88B

X-ray diffraction (XRD)

The structure of Fe-MIL-88B was investigated using powder X-ray diffraction (PXRD). The obtained pattern is similar to the simulated pattern calculated from the previous reports [19], with sharp identified peaks confirming the high crystalline of the MOF. The XRD pattern for Alen@β-CD@Fe-MIL-88B is similar to Fe-MIL-88B-NH_2 confirming that drug loading and incorporation into the MOF pores does not alter the framework structure. In this case, a slight decrease in peak intensity was observed, which

[Downloaded from ajpr.umsha.ac.ir on 2026-11-15]

[DOI: 10.53208/ajpr.6.2.88]

may be attributed to the amorphous state of the drug-loaded into the crystalline pores of MOF.

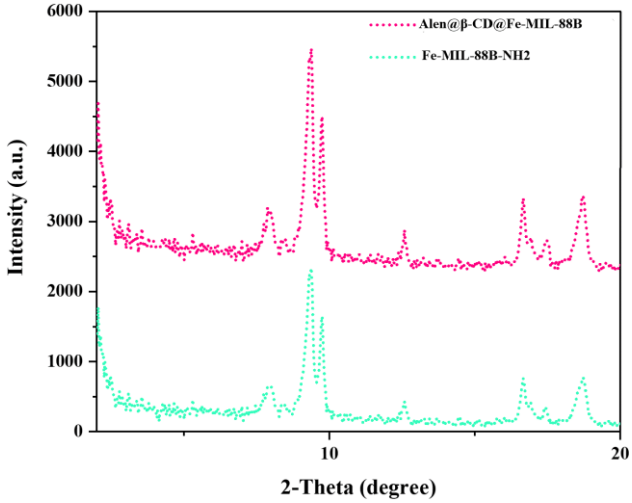


Figure 2. XRD patterns of Fe-MIL-88B-NH_2 and Alen@β-CD@Fe-MIL88B

Scanning Electron Microscopy (SEM)

Scanning electron microscopy (SEM) was employed to visualize the surface morphology of the Alen@β-CD@Fe-MIL-88B particles. Figure 3 reveals a densely packed, granular architecture composed of predominantly spheroidal particles with a relatively narrow size distribution. The particles exhibit a uniform, slightly textured surface and appear to be aggregated into loose clusters. The average particle diameter was determined to be approximately 50 nm, with a standard deviation of ± 10 nm, indicating a relatively narrow particle-size distribution.

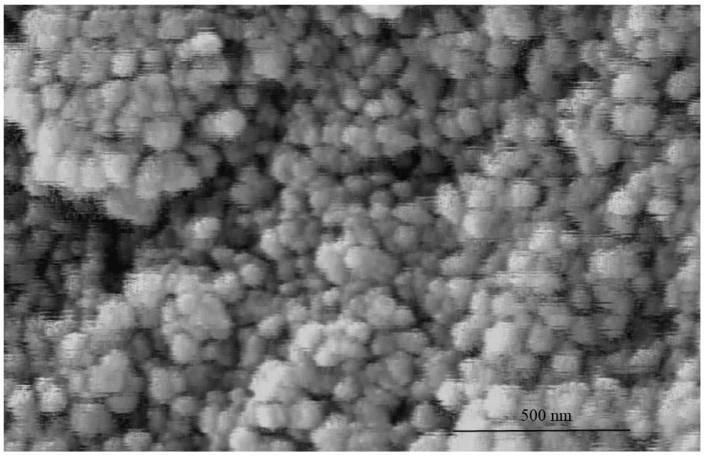


Figure 3. SEM image of Alen@β-CD@Fe-MIL88B

Scanning electron microscopy of PLLA/Alen@β-CD@Fe-MIL-88B scaffold

The SEM images of PLLA/Alen@β-CD@Fe-MIL-88B scaffold nanofibers are shown in Figure 4 Surface morphology of the PLLA/Alen@β-CD@Fe-MIL-88B nanofibrous scaffold was examined by scanning electron microscopy (SEM). The micrographs reveal a continuous, randomly oriented, and bead-free nanofibrous architecture in which individual fibers with diameters ranging from several hundred nanometers to a few micrometers assemble into a three-dimensional, highly interconnected porous network. The inter-fiber voids are uniformly distributed and may provide space for cell infiltration, nutrient transport, and tissue ingrowth. Furthermore, the fiber surfaces exhibit a uniform and slight increase in surface roughness, indicating favorable dispersion of

[Downloaded from ajpr.umsha.ac.ir on 2026-11-15]

[DOI: 10.53208/ajpr.6.2.88]

Alen@β-CD@Fe-MIL-88B particles within the polymeric matrix without the formation of undesirable agglomerates. In addition, image analysis of the PLLA/Alen@β-CD@Fe-MIL-88B nanofibers by ImageJ software showed a mean diameter of 500 ± 150 nm, indicating a relatively uniform diameter distribution and favorable reproducibility of the electrospinning process [22].

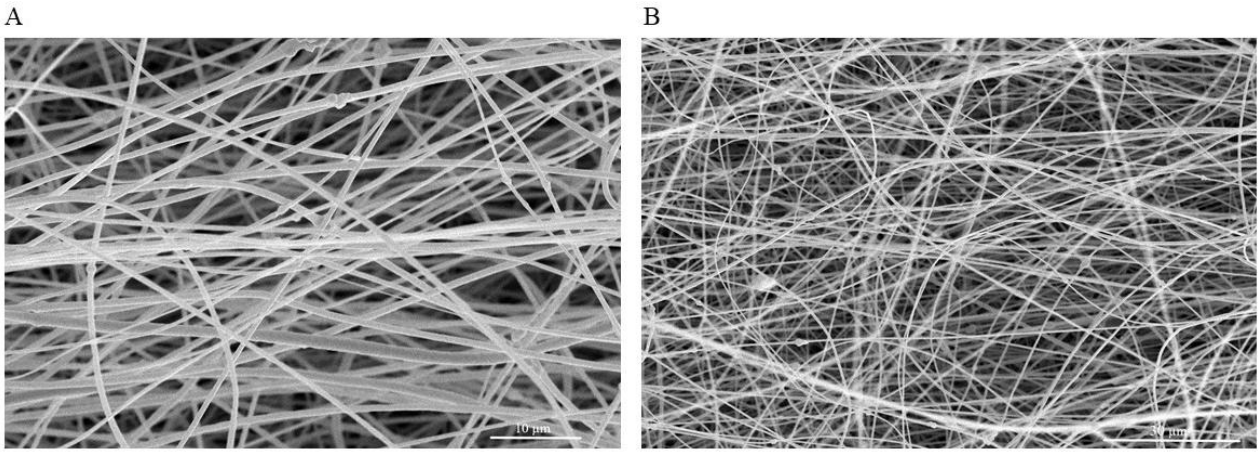


Figure 4. SEM images of PLLA/Alen@β-CD@Fe-MIL88B scaffold

Release study

The cumulative in vitro release profile of Alen from the composite scaffold was evaluated under physiological conditions (phosphate-buffered saline, pH 7.4) over a 21-day period (Figure 5). The release pattern exhibited a biphasic kinetics, characterized by an initial burst phase followed by a sustained release phase. Specifically, the Alen@β-CD@Fe-MIL-88B-loaded PLLA scaffold demonstrated a gradual and controlled release profile, with the cumulative drug release increasing steadily up to day 21. The nanoparticle-loaded PLLA scaffold displayed an initial burst release within the first 48 h, during which approximately 23% of the total loaded Alen was released within the first 48 h. This initial burst is attributed to the rapid dissolution of drug molecules that are weakly adsorbed onto the external surface of the scaffold or entrapped within superficial pores, which are readily accessible to the release medium. Subsequently, a sustained release phase ensued, reaching a plateau point at approximately 7 days after the start of release. This prolonged and controlled release behavior is advantageous for bone regeneration applications, as it ensures a sustained local therapeutic concentration of Alen, potentially enhancing osteogenic differentiation and new bone formation over an extended period.

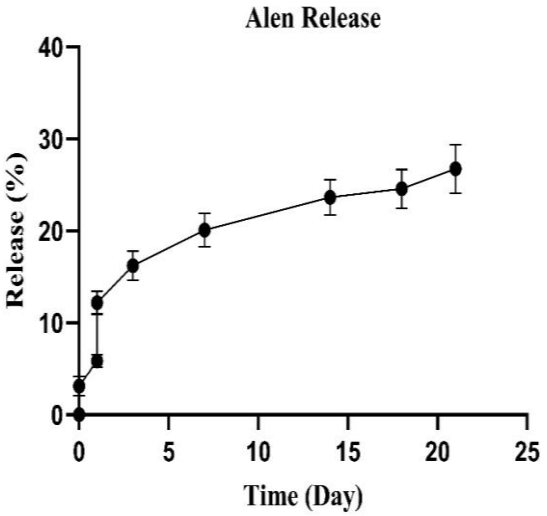


Figure 5. The cumulative controlled release profile of Alen from the composite scaffold at 37 °C and pH = 7.4. (Mean ± SD, n >3)

In vitro studies

Cell proliferation assay

The MTT assay revealed that all scaffold groups maintained cell viability above 85% over 3 days, confirming adequate biocompatibility. Pristine PLLA and PLLA/β-CD@Fe-MIL-88B (drug-free) supported normal cell proliferation, with viabilities reaching 105-106 % by day 3. In contrast, the alendronate-loaded scaffold (PLLA/Alen@β-CD@Fe-MIL-88B) exhibited a time-dependent decrease in viability from 92% (day 1) to 87% (day 3), attributed to the sustained

[Downloaded from ajpr.umsha.ac.ir on 2026-11-15]

[DOI: 10.53208/ajpr.6.2.88]

release of the bisphosphonate drug. Nevertheless, all values remained well above the 70% acceptability threshold (ISO 10993-5), indicating that the system combines therapeutic drug delivery with acceptable cytocompatibility for bone regeneration applications. Previous investigations have demonstrated that the cytotoxic response is concentration-dependent with respect to Alen. Specifically, Alen was found to elicit cytotoxic effects only when its concentration exceeded the threshold of 10^{-6} M, as reported in earlier studies [23, 24].

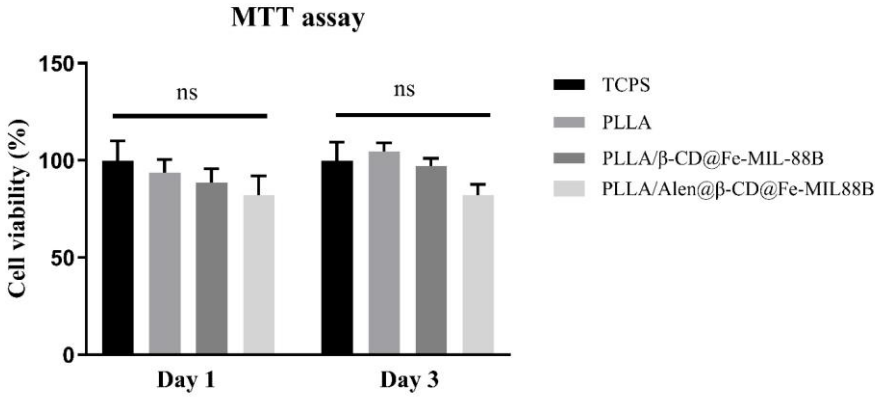


Figure 6. Evaluation of in-vitro cell cytotoxicity by MTT assay after 1 and 3 days of cell growth

Osteogenic differentiation

Alkaline Phosphatase (ALP) activity

ALP activity, an early osteogenic differentiation marker, was assessed over 7 and 14 days (Figure 7). The scaffold groups containing particles showed higher ALP levels than TCPS at both time points. The elevated ALP in the drug-loaded scaffold is attributed to the sustained release of Alen, which promotes osteoblast differentiation and matrix mineralization while inhibiting osteoclast activity. On day 14, the PLLA/Alen@β-CD@Fe-MIL-88B scaffold induced a statistically significant enhancement in ALP activity compared with the TCPS and PLLA scaffolds (***P < 0.0001) as well as the PLLA/β-CD@Fe-MIL-88B scaffold (*P < 0.05). This superior osteogenic response may be ascribed to the concurrent release of Alen from the Alen-loaded PLLA nanofibers. Consistent with these findings, previous investigations have established that Alen is capable of upregulating ALP activity, thereby promoting osteoblastic differentiation [25, 26]. Notably, the MOF-containing scaffold without drug also enhanced ALP activity, likely due to the high surface area of the nanoparticles and potential to adsorb extracellular proteins, thereby creating a favorable microenvironment for cell adhesion and osteogenic signaling [27]. The lower ALP value for pristine PLLA at day 14 suggests that while the polymer matrix is cytocompatible, it benefits from the bioactive nanoparticles and drug release to fully stimulate osteogenic commitment.

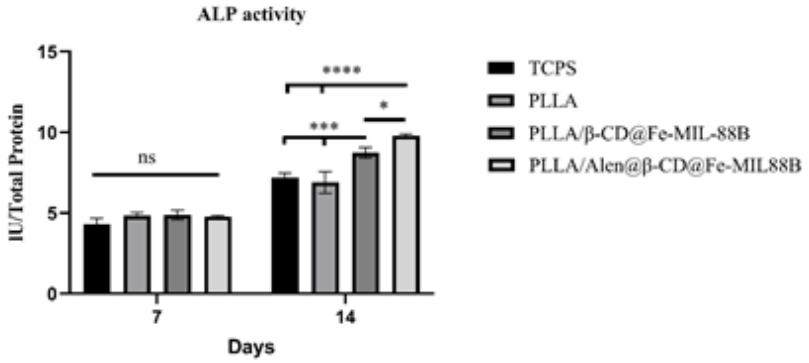


Figure 7. Effect PLLA scaffold and scaffolds containing NPs on ALP activity by hASCs at days 7 and 14. Results were expressed as a mean±SD, (*P < 0.05, **P < 0.01, ***P < 0.001, ****P < 0.0001)

[Downloaded from ajpr.umsha.ac.ir on 2026-11-15]

[DOI: 10.53208/ajpr.6.2.88]

Calcium content

Calcium deposition, a late-stage marker of osteogenic differentiation and extracellular matrix mineralization, was quantified over 7 and 14 days of culture (Figure 8). As expected, all groups exhibited a time-dependent increase in calcium content from day 7 to day 14, reflecting progressive matrix maturation.

On day 7, calcium deposition values showed no substantial differences among the groups. By day 14, a marked increase was observed across all samples. Notably, the MOF-containing scaffold with drug (PLLA/Alen@β-CD@Fe-MIL-88B) exhibited the highest calcium content, slightly surpassing TCPS, PLLA, and PLLA/β-CD@Fe-MIL-88B scaffolds. The higher, but not statistically significant, calcium deposition (day 14) in the PLLA/β-CD@Fe-MIL-88B group is attributed to the bioactive nature of the β-CD@Fe-MIL-88B nanoparticles, which provide a high surface area for protein adsorption and may facilitate nucleation of calcium phosphate minerals, thereby enhancing matrix mineralization [27]. The drug-loaded scaffold (PLLA/Alen@β-CD@Fe-MIL-88B) exhibited substantial calcium deposition, which was not statistically significant on day 7 but became significant by day 14, confirming that the sustained release of alendronate supports osteogenic differentiation, as previously indicated by ALP activity. Therefore, consistent with previous reports, the presence of Alen resulted in markedly elevated calcium deposition and ALP activity in the treated groups relative to the control groups, indicating a pronounced pro-osteogenic effect [15]. The lower calcium content in pristine PLLA (day 14) compared to the modified scaffolds suggests that the presence of nanoparticles and drug release collectively promote more robust extracellular matrix mineralization.

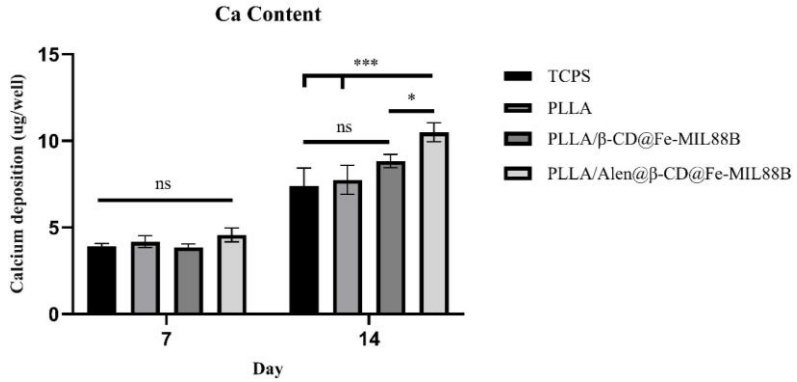


Figure 8. Effect of the PLLA scaffold and scaffolds containing NPs on Ca deposition by hASCs at days 7 and 14. Results are expressed as a mean ± SD, (*P < 0.05 and ***P < 0.001)

Conclusions

In summary, Fe-MIL-88B, as a flexible metal–organic framework (MOF), was successfully synthesized. To enhance the loading capacity of sodium alendronate, the surface of Fe-MIL-88B was modified with β-cyclodextrin (β-CD) through both physical and chemical interactions. The electrospinning method was utilized for the fabrication of PLLA, PLLA/β-CD@Fe-MIL-88B, and PLLA/Alen@β-CD@Fe-MIL-88B scaffolds. The PLLA scaffold containing Alen@β-CD@Fe-MIL-88B showed controlled Alen release over 21 days and can act as a local-dual delivery system. The PLLA/β-CD@Fe-MIL-88B and PLLA/Alen@β-CD@Fe-MIL-88B scaffolds compared to the TCPS showed not significant cytotoxicity. The PLLA/Alen@β-CD@Fe-MIL-88B scaffold promoted in vitro osteogenesis of hASCs. It can be concluded that PLLA/Alen@β-CD@Fe-MIL-88B scaffold is promising local-dual delivery systems and suitable candidates for the regeneration of bone tissue.

[Downloaded from ajpr.umsha.ac.ir on 2026-11-15]

[DOI: 10.53208/ajpr.6.2.88]

Acknowledgements

The authors would like to thank all individuals who contributed to this study. This research did not receive any specific grant from funding agencies in the public, commercial, or not-for-profit sectors.

Competing Interests

The authors declare that they have no competing interests.

References

1. Niu Z, Fan Y, Yin L, Tong Y, Yao L, Ding S, et al. Advancing nanomedicine: for bone defect repair and regeneration. Int J Nanomedicine. 2025;20:15043-15062. [DOI: 10.2147/IJN.S545353] [PMID] [PMCID]
2. Darchin Tabrizi F, Doosti-Telgerd M, Forouzideh N, Naghshnejad F, Seyedjafari E, Akbari Javar H, et al. Cinnamaldehyde/cinnamon essential oil loaded poly-L-lactic acid/hydroxyapatite fibrous scaffolds as osteogenic differentiation enhancing system for bone tissue engineering applications. J Biol Eng. 2025;19(1):84. [DOI: 10.1186/s13036-025-00547-3] [PMID] [PMCID]
3. Rahnamafar R, Moradikhah F, Doosti-Telgerd M, Oveisi M, Yousefi I, Moradi L, et al. Fine-tuning of hydrophilic properties of asymmetrically porous poly(ε-caprolactone)-based nanofibrous scaffolds containing dexamethasone for bone tissue engineering applications. J Appl Polym Sci. 2025;142(12):e56627. [DOI: 10.1002/app.56627]
4. Doosti-Telgerd M, Mahdavi FS, Moradikhah F, Porgham Daryasari M, Bayrami Atashgah R, Dolatyar B, et al. Nanofibrous scaffolds containing hydroxyapatite and microfluidic-prepared polyamidoamin/BMP-2 plasmid dendriplexes for bone tissue engineering applications. Int J Nanomedicine. 2020;15:2633-2646. [DOI: 10.2147/IJN.S244416] [PMID] [PMCID]
5. Sarkar C, Chowdhuri AR, Garai S, Chakraborty J, Sahu SK. Three-dimensional cellulose-hydroxyapatite nanocomposite enriched with dexamethasone loaded metal-organic framework: a local drug delivery system for bone tissue engineering. Cellulose. 2019;26(12):7253-7269. [DOI: 10.1007/s10570-019-02618-3]
6. Lim HC, Nam OH, Kim MJ, El-Fiqi A, Yun HM, Lee YM, et al. Delivery of dexamethasone from bioactive nanofiber matrices stimulates odontogenesis of human dental pulp cells through integrin/BMP/mTOR signaling pathways. Int J Nanomedicine. 2016;11:2557-2567. [DOI: 10.2147/IJN.S97846] [PMID] [PMCID]
7. Ma M, Noei H, Mienert B, Niesel J, Bill E, Muhler M, et al. Iron metal-organic frameworks MIL-88B and NH2-MIL-88B for the loading and delivery of the gasotransmitter carbon monoxide. Chemistry. 2013;19(21):6785-6790. [DOI: 10.1002/chem.201201743] [PMID]
8. Kang Z, Fan L, Sun D. Recent advances and challenges of metal-organic framework membranes for gas separation. J Mater Chem A. 2017;5(21):10073-10091. [DOI: 10.1039/C7TA01142C]
9. Li B, Wen HM, Zhou W, Chen B. Porous metal-organic frameworks for gas storage and separation: what, how, and why? J Phys Chem Lett. 2014;5(20):3468-3479. [DOI: 10.1021/jz501586e] [PMID]
10. Huang YB, Liang J, Wang XS, Cao R. Multifunctional metal-organic framework catalysts: synergistic catalysis and tandem reactions. Chem Soc Rev. 2017;46(1):126-157. [DOI: 10.1039/C6CS00250A] [PMID]
11. Della Rocca J, Lin W. Nanoscale metal-organic frameworks: magnetic resonance imaging contrast agents and beyond. Eur J Inorg Chem. 2010;2010(24):3725-3734. [DOI: 10.1002/ejic.201000496]
12. Ray Chowdhuri A, Bhattacharya D, Sahu SK. Magnetic nanoscale metal organic frameworks for potential targeted anticancer drug delivery, imaging and as an MRI contrast agent. Dalton Trans. 2016;45(7):2963-2973. [DOI: 10.1039/C5DT03736K] [PMID]
13. Wu MX, Yang YW. Metal-organic framework (MOF)-based drug/cargo delivery and cancer therapy. Adv Mater. 2017;29(23):1606134. [DOI: 10.1002/adma.201606134] [PMID]
14. Ma M, Bétard A, Weber I, Al-Hokbany NS, Fischer RA, Metzler-Nolte N. Iron-based metal-organic frameworks MIL-88B and NH2-MIL-88B: high quality microwave synthesis and solvent-induced lattice "breathing". Cryst Growth Des. 2013;13(6):2286-2291. [DOI: 10.1021/cg301738p]
15. Duque G, Rivas D. Alendronate has an anabolic effect on bone through the differentiation of mesenchymal stem cells. J Bone Miner Res. 2007;22(10):1603-1611. [DOI: 10.1359/jbmr.070701] [PMID]
16. Rodan GA, Fleisch HA. Bisphosphonates: mechanisms of action. J Clin Invest. 1996;97(12):2692-2696. [DOI: 10.1172/JCI118722] [PMID] [PMCID]
17. Bai SB, Liu DZ, Cheng Y, Cui H, Liu M, Cui MX, et al. Osteoclasts and tumor cells dual targeting nanoparticle to treat bone metastases of lung cancer. Nanomedicine. 2019;21:102054. [DOI: 10.1016/j.nano.2019.102054] [PMID]
18. Hochdörffer K, Abu Ajaj K, Schäfer-Obodozie C, Kratz F. Development of novel bisphosphonate prodrugs of doxorubicin for targeting bone metastases that are cleaved pH dependently or by cathepsin B: synthesis, cleavage properties, and binding properties to hydroxyapatite as well as bone matrix. J Med Chem. 2012;55(17):7502-7515. [DOI: 10.1021/jm300493m] [PMID]

[Downloaded from ajpr.umsha.ac.ir on 2026-11-15]

[DOI: 10.53208/ajpr.6.2.88]

19. Golmohamadpour A, Bahramian B, Shafiee A, Ma'mani L. Slow released delivery of alendronate using β-cyclodextrine modified Fe-MOF encapsulated porous hydroxyapatite. J Inorg Organomet Polym Mater. 2018;28(5):1991-2000. [DOI: 10.1007/s10904-018-0871-2]
20. Daryasari MP, Dusti Telgerd M, Karami MH, Zandi-Karimi A, Akbarijavar H, Khoobi M, et al. Poly-l-lactic acid scaffold incorporated chitosan-coated mesoporous silica nanoparticles as pH-sensitive composite for enhanced osteogenic differentiation of human adipose tissue stem cells by dexamethasone delivery. Artif Cells Nanomed Biotechnol. 2019;47(1):4020-4029. [DOI: 10.1080/21691401.2019.1658594] [PMID]
21. Wang Y, Cui W, Zhao X, Wen S, Sun Y, Han J, et al. Bone remodeling-inspired dual delivery electrospun nanofibers for promoting bone regeneration. Nanoscale. 2019;11(1):60-71. [DOI: 10.1039/C8NR07329E] [PMID]
22. Zhang Y, Wang QS, Yan K, Qi Y, Wang GF, Cui YL. Preparation, characterization, and evaluation of genipin crosslinked chitosan/gelatin three-dimensional scaffolds for liver tissue engineering applications. J Biomed Mater Res A. 2016;104(8):1863-1870. [DOI: 10.1002/jbm.a.35717] [PMID]
23. Correia VFP, Caldeira CL, Marques MM. Cytotoxicity evaluation of sodium alendronate on cultured human periodontal ligament fibroblasts. Dent Traumatol. 2006;22(6):312-317. [DOI: 10.1111/j.1600-9657.2005.00434.x] [PMID]
24. Sun J, Song F, Zhang W, Sexton BE, Windsor LJ. Effects of alendronate on human osteoblast-like MG63 cells and matrix metalloproteinases. Arch Oral Biol. 2012;57(6):728-736. [DOI: 10.1016/j.archoralbio.2011.12.007] [PMID]
25. Yun YP, Kim SJ, Lim YM, Park K, Kim HJ, Jeong SI, et al. The effect of alendronate-loaded polycarprolactone nanofibrous scaffolds on osteogenic differentiation of adipose-derived stem cells in bone tissue regeneration. J Biomed Nanotechnol. 2014;10(6):1080-1090. [DOI: 10.1166/jbn.2014.1819] [PMID]
26. Wang CZ, Chen SM, Chen CH, Wang CK, Wang GJ, Chang JK, et al. The effect of the local delivery of alendronate on human adipose-derived stem cell-based bone regeneration. Biomaterials. 2010;31(33):8674-8683. [DOI: 10.1016/j.biomaterials.2010.07.096] [PMID]
27. Xu C, Kang Y, Guan S, Dong X, Jiang D, Qi M. Iron-based metal-organic framework as a dual cooperative release system for enhanced vascularization and bone regeneration. Chin Chem Lett. 2023;34(5):107825. [DOI: 10.1016/j.cclet.2022.107825]

[Downloaded from ajpr.umsha.ac.ir on 2026-11-15]

[DOI: 10.53208/ajpr.6.2.88]